Scientific Research Publishing

Journal of Minerals and Materials Characterization and Engineering, 2024, 12, 334-345
https://www.scirp.org/journal/jmmce
ISSN Online: 2327-4085
ISSN Print: 2327-4077

# Revolutionizing Material Boundaries: High-Performance Diamond-Coated Steel via Long-Term MPCVD

**Angela Davis[1], Clyde Varner II[1*], Leslie Wilson[2], Padmaja Guggilla[1]**

[1]Department of Physics, Chemistry and Mathematics, College of Engineering, Technology and Physical Sciences, Alabama A&M University, Normal, AL, USA
[2]Center for Nanophase Materials Sciences, Oak Ridge National Laboratory, Oak Ridge, TN, USA
Email: *clyde.varner@aamu.edu

**How to cite this paper:** Davis, A., Varner II, C., Wilson, L. and Guggilla, P. (2024) Revolutionizing Material Boundaries: High-Performance Diamond-Coated Steel via Long-Term MPCVD. *Journal of Minerals and Materials Characterization and Engineering*, **12**, 334-345.
https://doi.org/10.4236/jmmce.2024.126021

**Received:** July 26, 2024
**Accepted:** November 10, 2024
**Published:** November 13, 2024



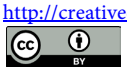



## Abstract

This research explores Microwave Plasma Chemical Vapor Deposition (MPCVD) for depositing diamond films on steel alloys (316L, 4140, and 1018) with a vanadium carbide interlayer to enhance adhesion and compatibility. The study reveals that a soft vanadium carbide interlayer and the FCC lattice match lead to a Ta-C film. The results of the graphite inhibition and diamond deposition varied with the steel alloy underlayer composition. In the 316L steel alloy, we successfully formed a thick, compressive strain-induced, sp3-bonded tetrahedral amorphous carbon layer without graphite. The findings have wide-ranging applications in environments demanding high durability and thermal conductivity.

## Keywords

MPCVD (Microwave Plasma Chemical Vapor Deposition), Raman Spectroscopy, Steel Alloys (316L, 4140, 1018), Coatings, Chip-Resistance

## 1. Introduction

Diamond films, with their exceptional set of properties—ranging from extreme hardness and high thermal conductivity to electrical resistivity—have garnered significant attention in scientific research and technological advancements. [1]-[4] These extraordinary features make diamond films a material of choice for a plethora of industrial and scientific applications, such as cutting tools, thermal management systems, semiconductor devices, and even optoelectronic components [5] [6]. Among the various methodologies for synthesizing diamond films,

Microwave Plasma Chemical Vapor Deposition (MPCVD) has emerged as a particularly effective and versatile technique, significantly propelling the field towards new frontiers. [7]-[9] The selection of an appropriate substrate material is a pivotal factor in the successful deposition of diamond films. While silicon substrates have been a traditional choice owing to their well-understood properties and compatibility with diamond, the focus has gradually shifted toward alloys. [10]-[12] Fe-based alloys such as 316, 1018, and 4140 are commonly used in structural applications. These alloys offer a combination of high strength, good corrosion resistance, and excellent mechanical properties. Fe-based amorphous/nanocrystalline alloys, for example, exhibit high saturation magnetic flux density (Bs), high permeability, low coercivity (Hc), and low magnetostriction, making them suitable for use in distribution transformers, reactors, and other devices [13]. Fe-based superelastic alloys are also widely used due to their low cost, easy processing, good plasticity and toughness, and wide applicable temperature range. They find applications in machinery, aerospace, transmission, and medicine [14]. Fe-based amorphous materials, on the other hand, offer opportunities for magnetic sensors, actuators, and magnetostrictive transducers due to their high saturation magnetostriction and low coercive field [15]. However, the intrinsic differences in physical and chemical properties between diamond and steel alloys often necessitate the use of an interlayer to enhance adhesion and compatibility [16]-[18]. Raman spectroscopy serves as an invaluable analytical tool in this context, offering insights into the quality, phase composition, and even the defect structure of the diamond films [19] [20]. Nonetheless, the interpretation of Raman spectra is not straightforward and can be affected by a myriad of factors, such as deposition pressure, gas composition, and plasma power during the MPCVD process, making it essential to carefully control and understand these variables [21]. The objective of this investigation is multifaceted. Primarily, it aims to meticulously analyze the Raman spectra of diamond films deposited on 316, 1018, and 4140 steel alloys via MPCVD. A special focus is accorded to the role of Vanadium Carbide (VC) interlayers, exploring how they influence the quality, adhesion, and compatibility of the diamond films with the steel substrates. This investigation extends beyond the boundaries of material science and engineering, positioning itself at the convergence of addressing global challenges and catalyzing advancements in emerging technologies. By harnessing Microwave Plasma Chemical Vapor Deposition (MPCVD) for the development of diamond-coated steel alloys, we illuminate pathways toward sustainable manufacturing practices, offering solutions that promise enhanced durability and thermal efficiency. Such innovations hold the potential to revolutionize sectors ranging from electronics—where the demand for heat management solutions grows alongside the miniaturization of devices—to renewable energy technologies, where efficiency and longevity are paramount. Moreover, the application of this research in biomedical engineering, through the development of biocompatible and durable materials, underscores its multifaceted impact. By articulating these connections, this work not only broadens

its appeal to a diverse peer community but also underscores its contribution to a sustainable future, inviting interdisciplinary collaboration and exploration across scientific and technological domains.

## 2. Methodology

The recipe for nanocrystalline diamond synthesis has been published previously elsewhere [22]. Nanocrystalline diamond films were synthesized using the DiamoTek 700-6 Microwave Plasma CVD system from Microwave Enterprises, Ltd. "1" diameter steel substrates of alloys 316SS, 4140 steel, and Low carbon steel (1018) were employed. Both 5 mm thick CeraTough-0401: Vanadium Carbonitride (VCN) and 0.5 mm thick Hot Thermo-diffused VC coated 316SS, 4140, and Low Carbon Steel (1018) were all purchased from IBC Coatings, Inc. and used as is.

Prior to deposition, the coated substrates were seeded with a diamond slurry in methanol containing 0.005 g of diamond nano-powder with an approximate size of 3.2 nm.

The film growth process was initiated by igniting a microwave plasma with a power of 6 kW at a frequency of 2.45 GHz. The plasma consisted of a mixture of $H_2$, $CH_4$, and Ar feeding gases. The chamber operated at a pressure range of 40 to 105 Torr. These variables—gas ratios, microwave power, and chamber pressure—served as the key parameters for controlling the grain size in the resulting films. Specifically, the nanocrystalline diamond was grown using a gas mixture of 2.45% $CH_4$, 90% Ar, and 7.55% $H_2$ at a chamber pressure and microwave power set at 105 Torr and 1330 W, respectively.

For characterization, Raman spectroscopy measurements were performed using a Renishaw InVia Raman microscope with a 633 nm light source. Additionally, scanning electron microscopy (SEM) images were captured using a Thermo Fischer Scientific Nova 600 NanoLab and the Carl Zeiss Merlin FE-SEM to confirm the diamond film thickness and compare film morphologies.

## 3. Results and Discussion

VCN failed to show any result after diamond deposition. Therefore, this analysis is for Long Diamond Microwave Plasma Chemical Vapor Deposition on Vanadium Carbide interlayer was tested directly on 316 L, 1018, and 4140 substrates since the vanadium carbide interlayer thickness was ~.5 mm the distance between the steel alloy substrate is increased to prevent the initiation of a ~20 um thick and sp3-bonded tetrahedral amorphous carbon (ta-C) coating Diamond and rapid carbon diffusion into the substrate and the preferential formation of an intermediate graphite layer on steel surface catalyzed by iron and nickel in the substrate.

Figure (A1, SI) Shows coated VCN (top) and VC (bottom) coated steel surface before deposition. In **Figure A2**, a clear deposition of VCN-coated samples delaminated after long MPCVD diamond deposition. Raman spectra will be discussed in **Figure 2**. In **Figure A2** and **Figure A3**, 4140 VC coated steel shows that during the growth process, a diamond film occurs on the top of the graphite,

which has separated the diamond from the steel substrate.

As depicted in the SEM comparison, Figure 1, we examine the surface transformations of SS316L and Silicon substrates layered with VC, following the CVD process. On the VC-laden SS316 substrate, the diamond structures in nature after extended CVD processing (27 hours). This implies a robust barrier effect of the 500-micron VC interlayer against carbon-metal interdiffusion. The thickness of the resultant film is ~ 20 um. Figure 1 right, shows the silicon substrates distinct formation of diamond nanocrystallites, indicating a re-nucleation pathway of diamond film formation. From the difference in the images, it can be determined on silicon, the clear diamond nanocrystallites (Figure 1, right) that can coalesce quickly to form microcrystalline diamond thin films, as seen in the 316L SS diamond-coated image (Figure 1, left).

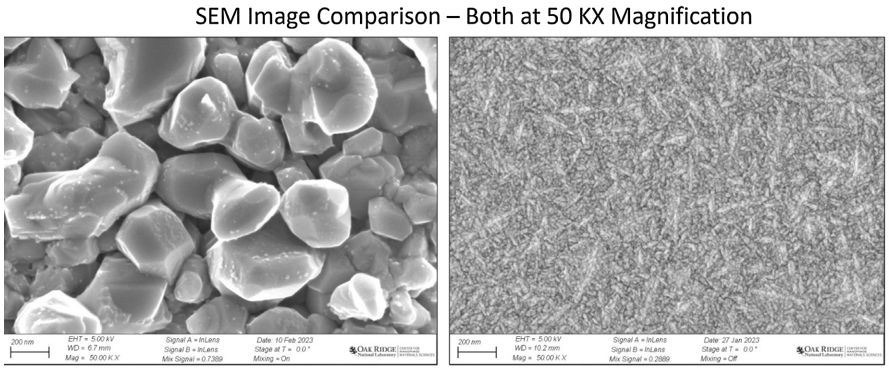


Figure 1. SEM comparison of 27 hours MPCVD of diamond 316 (left) and 4 hours 22 minutes MPCVD of diamond on silicon substrate control sample (right).

Figure A4 illustrates the delamination phenomena observed in diamond samples post-MPCVD on VCN-coated steel. An intriguing aspect of these images is the observed partial detachment of the VCN interlayer alongside the diamond film, despite expectations of a 32-micron diamond layer from linear deposition models.

The D band and G Band shifts and FWHM can be found in the supplementary data (Figure A5 and Figure A6). The Raman spectrum analysis in Figure 2 shows an overlay of short-term ~2 hours inhomogeneously broadened control small nanocrystalllite coated diamond silicon sample and nanocrystal growth coated steel alloys post a long-term MPCVD process. The silicon sample is broadened due to the many microstates of the smaller nanocrystallites, revealing the disorder evident in the D and G bands. The ratio of D/G gives the relative disorder of the diamond coating [23]. Particularly striking are the distinct diamond peaks at 1332 $cm^{-1}$ across 1018 and 4140 spectra and a unique, blue-shifted peak at ~1395 $cm^{-1}$ in the 316-steel diamond-coated spectra, likely indicating diverse bonding environments [24]. The peak height ratio in the 1018 sample points to suppressed graphitization and low disorder. In the 4140 coated steel samples, the Peak to Peak height ratio shows a large amount of graphitization and induced diamond disorder. The main blue shifted portion of the 316L SS spectra which is around 63.15 $cm^{-1}$ from the expected 1332 $cm^{-1}$. In order to determine the strain in the 316L SS diamond-coated

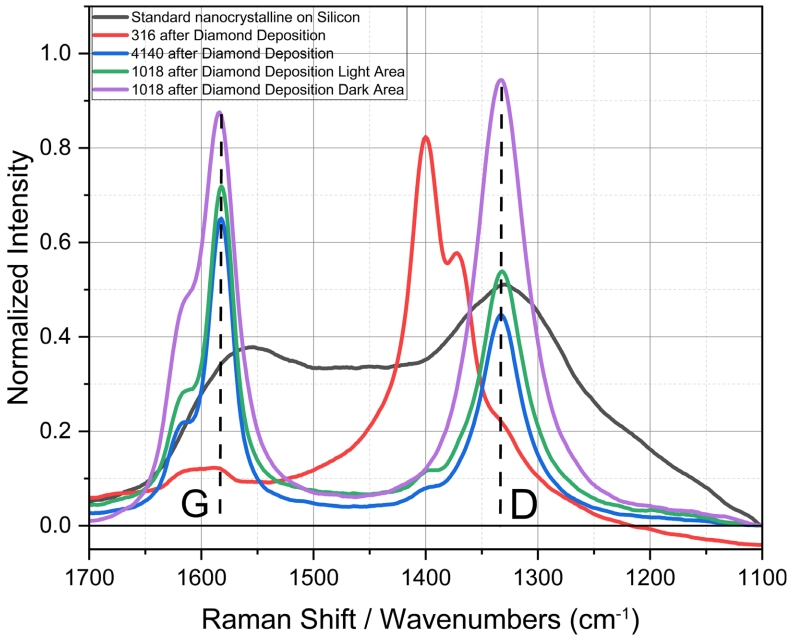


**Figure 2.** Raman spectrum of diamond coated with VC interlayer: 316 (red), 4140 (blue), 1018 (light area) (green), and 1018 (dark area) (purple) steel alloys after 27-hour long diamond deposition. The standard nanocrystalline diamond overlay is shown in black for comparison.

sample, we use the following equation:

$$\varepsilon_c = -\frac{\Delta\omega}{(\omega_0 \times \gamma)} \tag{1}$$

where:

- $\Delta\omega$ is the Raman shift (change in wavenumber)
- $\omega_0$ is the original wavenumber (unstrained)
- $\gamma$ is the Gruneisen parameter

We used this formula to calculate the strain for 316L SS, using 1332 $cm^{-1}$ for $\omega_0$ and 1.2 as $\gamma$, as has been reported for the Gruneisen parameter for diamonds [25] [26]. The calculated value for the strain using Equation (1) is −0.04% or −4%. This value corresponds to the $\Delta\omega$ = 63.15 $cm^{-1}$. The 316 SS spectra correspond to an extreme compressive strain, which is essentially tightening of the diamond matrix to a sp3-bonded tetrahedral amorphous carbon with an average calculated bond length of 1.479 Å. the introduction of strain in the first order Raman peak, is evident in the blueshift and splitting of the peak at ~1395 $cm^{-1}$ due to the transverse optical (TO) and longitudinal optical (LO) phonon modes (BZ) [27]. The extremely strained structural distortion induces relaxation of the q ≈ 0 BZ zone and allows detection of the phonon modes away from the first Brillouin zone [27]. Note the first order BZ peak as the small broad shoulder at the bottom of the low wavenumber side of the 316L SS Raman spectrum at 1332 $cm^{-1}$. The majority of diamonds have been grown to a high concentration due to re-nucleation and have compressively strained due to bonding with and the intrinsic nature of the softness of the thick VC interlayer top surface. The surface topology is a soft impression of

the supporting structural bonded bottom V-C layer and the steel surface. The ta-C is high quality by SEM and completely covers the diamond-like FCC 316L SS surface (Figure 1) with a sp3-bonded tetrahedral amorphous carbon coating (ta-C) of extreme strain. The extremely strong directional sp3 bonds lead to many extraordinary properties and applications of ta-C, such as the highest known hardness, very low friction and adhesion, unmatched thermal conductivity, electronic mobility, the highest electron dispersion, high dielectric breakdown, radiation hardness, biocompatibility, and chemical inertness. [28] [29] The graphitic peaks are at the background level and almost absent in the 316L SS coated Raman Spectrum, indicating that the formation of graphite has been prevented from being formed. This sample has been completely coated with a continuous and thick diamond cladding. This is advantageous, and it has surpassed the quality of the nanocrystalline standard sample. In the 1018 and 4140 spectra, Figure 2, the presence of sharp graphitic peaks at ~1620 $cm^{-1}$ point towards a complex interplay of $sp_3$ and $sp_2$ carbon structures [24]. The difference in diamond coating morphology is confirmed by the SEM image of the 4140 sample (A4, SI). Figure 3 shows the second-order phonon mode of graphite [30]. Graphitization and Disorder are the highest in the 4140-diamond-coated sample. The 4140 This spectral analysis provides insightful clues into the nature of the diamond films and the underlying carbide layer, especially in terms of graphite formation and its potential impact on film uniformity and adhesion.

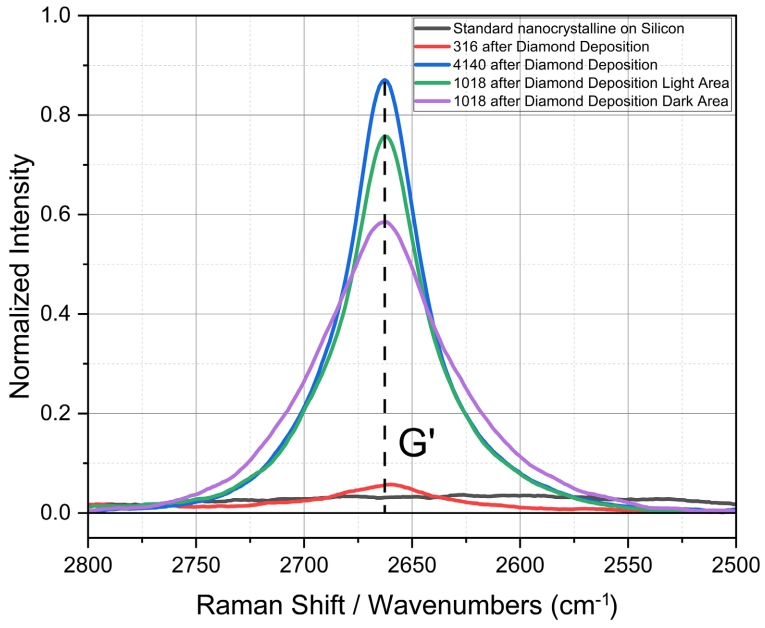


Figure 3. Raman spectrum of diamond coated with VC interlayer: 316 (red), 4140 (blue), 1018 (light area) (green), and 1018 (dark area) (purple) steel alloys after 27-hour long diamond deposition. The standard nanocrystalline diamond overlay is shown in black for comparison.

## 4. Conclusions

In this study, we unravel the intricate interplay between diamond deposition

variables and the resultant film qualities on steel alloys, underpinned by comprehensive Raman spectral analysis. Our findings illuminate the pivotal role of D and G band shifts in demarcating the crystallinity and disorder within carbon materials, a phenomenon that is intricately tied to the electronic, mechanical, and thermal properties of the resultant films. The nuanced understanding of D and G band behaviors, garnered through meticulous spectral analysis, provides a robust framework for tailoring material properties to specific application needs. This research not only advances the frontier of material science by offering a deeper insight into the structural nuances of diamond-coated steel alloys but also opens new avenues for innovation in fields as diverse as electronics, energy storage, and nanotechnology. By marrying the unique properties of diamond with the versatility of steel, we set the stage for next-generation materials that promise to revolutionize industrial applications, from enhancing the durability of mechanical parts to enabling more efficient thermal management solutions. Thus, our work stands at the confluence of fundamental science and practical technology, heralding a new era of materials engineering that leverages the full potential of composite materials for sustainable and high-performance applications.

The successful suppression of graphite formation in ta-C diamond films grown on 316L stainless steel, as compared to the results on diamond-coated 1018 and 4140 steel alloys, can be attributed to several key factors inherent to the composition and microstructure of 316L stainless steel. Notably, 316L is a low-carbon variant of the 316 stainless steel, typically containing less than 0.03% carbon. This low carbon content is crucial in reducing the formation of chromium carbide ($Cr_7C_3$ or $Cr_{23}C_6$) at grain boundaries, especially under the high-temperature conditions of Microwave Plasma Chemical Vapor Deposition (MPCVD). The minimized carbide formation at the interface between the steel and the vanadium carbide (VC) coating significantly reduces the likelihood of graphite nucleation, thereby promoting the growth of high-quality diamond films.

In addition to its low carbon content, 316L stainless steel contains high levels of chromium (16% - 18%), along with nickel (10% - 14%) and molybdenum (2% - 3%). The presence of chromium enhances the oxidation resistance of the alloy, which is vital for maintaining a stable interface with the VC coating during the MPCVD process. This stability is critical in suppressing graphite formation and facilitating diamond growth. The other alloying elements, such as nickel and molybdenum, contribute to the overall structural stability of the alloy, particularly under the extreme conditions of diamond film deposition.

Furthermore, the austenitic microstructure of 316L stainless steel, characterized by its face-centered cubic (FCC) crystal structure, provides a compatible and uniform lattice for the VC coating. This compatibility ensures a stable and conducive growth surface for ta-C diamond deposition. The thermal properties of 316L, including its conductivity and coefficient of thermal expansion, also play a significant role in determining the stress states at the interface during the MPCVD process, further influencing the diamond film's quality.

In contrast, 1018 and 4140 steels, with their higher carbon contents and lack of substantial chromium and nickel, offer favorable conditions for diamond growth. These differences in composition and microstructure lead to a higher tendency for diamond growth.

Overall, the unique combination of low carbon content, specific alloying elements, and austenitic microstructure in 316L stainless steel creates an optimal substrate for high-quality diamond film growth using MPCVD, effectively minimizing the risk of graphite formation and enhancing the diamond film's quality compared to 1018 and 4140 steels.

## Authors' Contributions

Clyde Varner II was involved in Conceptualization, Investigation, Data Curation, Visualization, Writing and Editing of the Manuscript. Leslie Wilson was involved in Investigation, Methodology and Data Curation, Writing and Editing the Manuscript. Angela Davis was involved in Editing of the Manuscript. Padmaja Guggilla was involved in Editing of the Manuscript.

## Funding

MPCVD, SEM, and Raman Spectroscopic Analysis research were conducted as part of a user project at the Center for Nanophase Materials Sciences (CNMS), which is a US Department of Energy, Office of Science User Facility at Oak Ridge National Laboratory.

This work was supported by the National Science Foundation under Grant No. #2331969. Any opinions, findings, conclusions, or recommendations expressed in this work are those of the author(s) and do not necessarily reflect the views of the National Science Foundation.

## Data Availability

Data will be made available upon request.

## Conflicts of Interest

The authors declare no conflicts of interest regarding the publication of this paper.

## References

[1] Auciello, O. and Aslam, D.M. (2021) Review on Advances in Microcrystalline, Nanocrystalline and Ultrananocrystalline Diamond Films-Based Micro/Nano-Electromechanical Systems Technologies. *Journal of Materials Science*, **56**, 7171-7230. https://doi.org/10.1007/s10853-020-05699-9

[2] Liu, X., Zhang, H., Lin, G., Wang, Z., Zhang, J. and Shi, H. (2023) Advances in Deposition of Diamond Films on Cemented Carbide and Progress of Diamond Coated Cutting Tools. *Vacuum*, **217**, Article 112562. https://doi.org/10.1016/j.vacuum.2023.112562

[3] Handschuh-Wang, S., Wang, T. and Tang, Y. (2021) Ultrathin Diamond Nanofilms—Development, Challenges, and Applications. *Small*, **17**, Article 2007529.

https://doi.org/10.1002/smll.202007529

[4] Xu, B. and Tian, Y. (2020) Diamond Gets Harder, Tougher, and More Deformable. *Matter and Radiation at Extremes*, **5**, Article 068103. https://doi.org/10.1063/5.0029519

[5] Rajasekaran, S., Abild-Pedersen, F., Ogasawara, H., Nilsson, A. and Kaya, S. (2013) Interlayer Carbon Bond Formation Induced by Hydrogen Adsorption in Few-Layer Supported Graphene. *Physical Review Letters*, **111**, Article 085503. https://doi.org/10.1103/physrevlett.111.085503

[6] Narayan, R.J., Boehm, R.D. and Sumant, A.V. (2011) Medical Applications of Diamond Particles & Surfaces. *Materials Today*, **14**, 154-163. https://doi.org/10.1016/s1369-7021(11)70087-6

[7] Kim, Y., Song, W., Lee, S.Y., Jeon, C., Jung, W., Kim, M., *et al.* (2011) Low-Temperature Synthesis of Graphene on Nickel Foil by Microwave Plasma Chemical Vapor Deposition. *Applied Physics Letters*, **98**, Article 263106. https://doi.org/10.1063/1.3605560

[8] Liang, Q., Yan, C., Lai, J., Meng, Y., Krasnicki, S., Shu, H., *et al.* (2014) Large Area Single-Crystal Diamond Synthesis by 915 MHz Microwave Plasma-Assisted Chemical Vapor Deposition. *Crystal Growth & Design*, **14**, 3234-3238. https://doi.org/10.1021/cg500693d

[9] Hong, S.P., Lee, K., You, H.J., Jang, S.O. and Choi, Y.S. (2022) Scanning Deposition Method for Large-Area Diamond Film Synthesis Using Multiple Microwave Plasma Sources. *Nanomaterials*, **12**, Article 1959. https://doi.org/10.3390/nano12121959

[10] Li, X., He, L., Li, Y. and Yang, Q. (2020) Diamond Deposition on Iron and Steel Substrates: A Review. *Micromachines*, **11**, Article 719. https://doi.org/10.3390/mi11080719

[11] Damm, D., Contin, A., Barbieri, F., Trava-Airoldi, V., Barquete, D. and Corat, E. (2017) Interlayers Applied to CVD Diamond Deposition on Steel Substrate: A Review. *Coatings*, **7**, Article 141. https://doi.org/10.3390/coatings7090141

[12] Kumar, N., Sankaran, K.J., Kozakov, A.T., Sidashov, A.V., Nicolskii, A.V., Haenen, K., *et al.* (2019) Surface and Bulk Phase Analysis of the Tribolayer of Nanocrystalline Diamond Films Sliding against Steel Balls. *Diamond and Related Materials*, **97**, Article 107472. https://doi.org/10.1016/j.diamond.2019.107472

[13] Zhou, J., You, J. and Qiu, K. (2022) Advances in Fe-Based Amorphous/Nanocrystalline Alloys. *Journal of Applied Physics*, **132**, Article 040702. https://doi.org/10.1063/5.0092662

[14] Li, Z., Zhang, Y., Dong, K. and Zhang, Z. (2022) Research Progress of Fe-Based Superelastic Alloys. *Crystals*, **12**, Article 602. https://doi.org/10.3390/cryst12050602

[15] Ozden, M.G. and Morley, N.A. (2021) Laser Additive Manufacturing of Fe-Based Magnetic Amorphous Alloys. *Magnetochemistry*, **7**, Article 20. https://doi.org/10.3390/magnetochemistry7020020

[16] Martins, R.L., Damm, D.D., Volu, R.M., Pinheiro, R.A., Rosa, F.M., Trava-Airoldi, V.J., *et al.* (2021) Laser Cladding of Vanadium Carbide Interlayer for CVD Diamond Growth on Steel Substrate. *Surface and Coatings Technology*, **421**, Article 127387. https://doi.org/10.1016/j.surfcoat.2021.127387

[17] Dass, A. and Moridi, A. (2019) State of the Art in Directed Energy Deposition: From Additive Manufacturing to Materials Design. *Coatings*, **9**, Article 418. https://doi.org/10.3390/coatings9070418

[18] Delfani-Abbariki, S., Abdollah-Zadeh, A., Hadavi, S.M.M., Abedi, M. and Derakh-

shandeh, S.M.R. (2018) Enhancing the Adhesion of Diamond-Like Carbon Films to Steel Substrates Using Silicon-Containing Interlayers. *Surface and Coatings Technology*, **350**, 74-83. https://doi.org/10.1016/j.surfcoat.2018.06.055

[19] Matsuoka, M., Tsuchida, Y., Ohtani, N., Yamada, T., Koizumi, S. and Shikata, S. (2021) Polarized Raman Spectroscopy of Phosphorous Doped Diamond Films. *Diamond and Related Materials*, **114**, Article 108283. https://doi.org/10.1016/j.diamond.2021.108283

[20] Polushin, N.I., Laptev, A.I., Shitareva, M.S., Muratov, D.S., Maslov, A.L., Kirichenko, A.N., *et al.* (2021) The Use of Spectroscopy Methods for Structural Analysis of CVD Diamond Films, Polycrystalline and Single-Crystal Diamonds. *MATEC Web of Conferences*, **336**, Article 01013. https://doi.org/10.1051/matecconf/202133601013

[21] Jian, X., Hu, J., Tang, J. and Ma, Q. (2021) Optimization of Deposition Parameters for MPCVD Diamond Coatings Grown on WC-Co Substrates Using the Taguchi and Analytical Hierarchy Process Methods. *Transactions of the Canadian Society for Mechanical Engineering*, **45**, 626-634. https://doi.org/10.1139/tcsme-2020-0148

[22] Saturday, L., Wilson, L., Retterer, S., Evans, N.J., Briggs, D., Rack, P.D., *et al.* (2021) Thermal Conductivity of Nano- and Micro-Crystalline Diamond Films Studied by Photothermal Excitation of Cantilever Structures. *Diamond and Related Materials*, **113**, Article 108279. https://doi.org/10.1016/j.diamond.2021.108279

[23] Akahama, Y. and Kawamura, H. (2006) Pressure Calibration of Diamond Anvil Raman Gauge to 310GPa. *Journal of Applied Physics*, **100**, Article 043516. https://doi.org/10.1063/1.2335683

[24] Li, Y.S., Tang, Y., Yang, Q., Xiao, C. and Hirose, A. (2010) Growth and Adhesion Failure of Diamond Thin Films Deposited on Stainless Steel with Ultra-Thin Dual Metal Interlayers. *Applied Surface Science*, **256**, 7653-7657. https://doi.org/10.1016/j.apsusc.2010.06.022

[25] Migliori, A., Ledbetter, H., Leisure, R.G., Pantea, C. and Betts, J.B. (2008) Diamond's Elastic Stiffnesses from 322K to 10K. *Journal of Applied Physics*, **104**, Article 053512. https://doi.org/10.1063/1.2975190

[26] Hess, P. (2012) The Mechanical Properties of Various Chemical Vapor Deposition Diamond Structures Compared to the Ideal Single Crystal. *Journal of Applied Physics*, **111**, Article 051101. https://doi.org/10.1063/1.3683544

[27] Pu, M., Zhang, F., Liu, S., Irifune, T. and Lei, L. (2019) Tensile-Strain Induced Phonon Splitting in Diamond. *Chinese Physics B*, **28**, Article 053102. https://doi.org/10.1088/1674-1056/28/5/053102

[28] Tan, L., Sheng, H., Lou, H., Cheng, B., Xuan, Y., Prakapenka, V.B., *et al.* (2020) High-pressure Tetrahedral Amorphous Carbon Synthesized by Compressing Glassy Carbon at Room Temperature. *The Journal of Physical Chemistry C*, **124**, 5489-5494. https://doi.org/10.1021/acs.jpcc.0c00247

[29] Zeng, Z., Yang, L., Zeng, Q., Lou, H., Sheng, H., Wen, J., *et al.* (2017) Synthesis of Quenchable Amorphous Diamond. *Nature Communications*, **8**, Article No. 322. https://doi.org/10.1038/s41467-017-00395-w

[30] Knight, D.S. and White, W.B. (1989) Characterization of Diamond Films by Raman Spectroscopy. *Journal of Materials Research*, **4**, 385-393. https://doi.org/10.1557/jmr.1989.0385

## Supplementary Information


**Figure A1.** VCN (top and VC (bottom) coated steel alloys after long MPVCVD diamond deposition.


**Figure A2.** VCN (top and VC (bottom) coated steel alloys after long MPVCVD diamond deposition.


**Figure A3.** Layout of diamond-coated steel samples with VC interlayer.

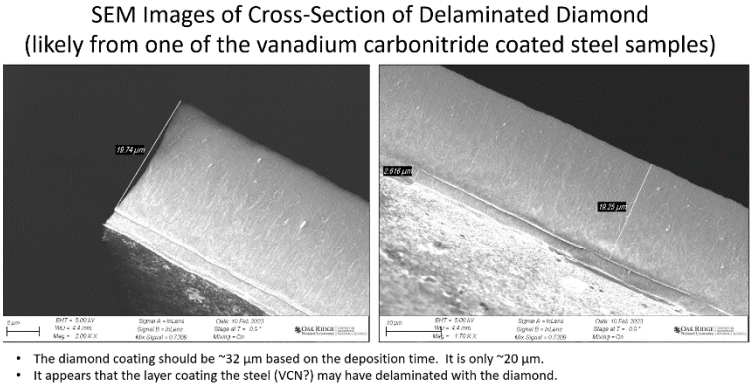


**Figure A4.** Two SEM images of delaminated diamond sample from VCN coated steel after 27-hour Long MPCVD Diamond Deposition, thickness ~20 microns.

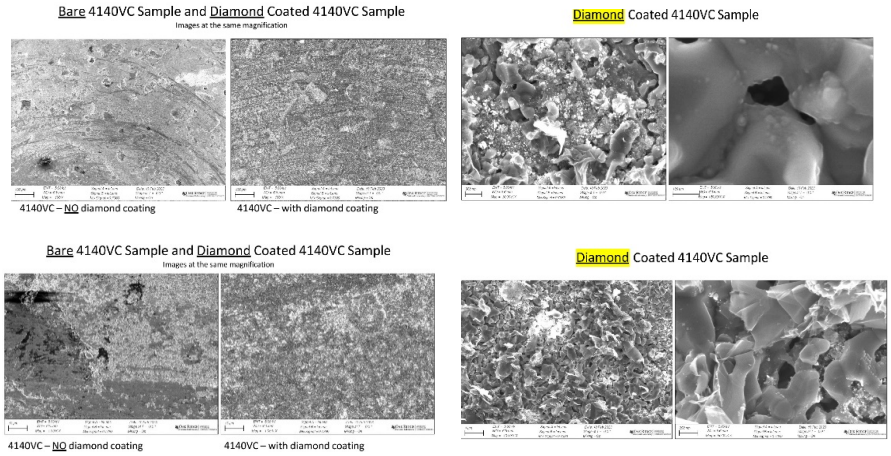


**Figure A5.** Various magnification comparisons show differences between diamond-coated VC-TDH and silicon-coated diamond control (magnification is increased clockwise for the four image pair comparisons).

| Sample Type | Band | Peak Position (cm^-1) | FWHM |
|---|---|---|---|
| Standard nanocrystalline on Silicon | D | 1330.37 | 233.53 |
| Standard nanocrystalline on Silicon | G | 1554.88 | 34.25 |
| 316 after Diamond Deposition | D | 1372.01 | 100 |
| 316 after Diamond Deposition | G | 1589.44 | 32.89 |
| 4140 after Diamond Deposition | D | 1333.35 | 28.1 |
| 4140 after Diamond Deposition | G | 1582.25 | 19.34 |
| 1018 after Diamond Deposition Light Area | D | 1331.86 | 29.34 |
| 1018 after Diamond Deposition Light Area | G | 1582.25 | 20.12 |
| 1018 after Diamond Deposition Dark Area | D | 1333.35 | 36.28 |
| 1018 after Diamond Deposition Dark Area | G | 1583.69 | 34.76 |

**Figure A6.** Peak position and FWHM for the D and G band.

| Sample Type | Band | Peak Position (cm^-1) | FWHM |
|---|---|---|---|
| Standard nanocrystalline on Silicon | G' | 2626.13 | 203.437 |
| 316 after Diamond Deposition | G' | 2660.28 | 36.8141 |
| 4140 after Diamond Deposition | G' | 2662.72 | 32.42464 |
| 1018 after Diamond Deposition Light Area | G' | 2662.72 | 33.93657 |
| 1018 after Diamond Deposition Dark Area | G' | 2662.72 | 54.19112 |

**Figure A7.** Peak position and FWHM for the G' band.